Electronic Supplementary Material (ESI) for Journal of Materials Chemistry A.
This journal is © The Royal Society of Chemistry 2025

Supplementary Information

Anion-engineered chalcogenide perovskites Ba_2HfCh_4: from light emitters to photovoltaics

Juan Du,*[a] Chenyi Yang,[a] Baoshan Zhu,[a] Chong Tian,[b] Junjie shi[b] and Congxin Xia*[c]

[a] *Department of Physics and Optoelectronic Engineering, Beijing University of Technology, Beijing 100124, China. E-mail:dujuan1121@bjut.edu.cn*

[b] *State Key Laboratory for Artificial Microstructures and Mesoscopic Physics, School of Physics, Peking University Yangtze Delta Institute of Optoelectronics, Peking University, Beijing 100871, China.*

[c] *School of Physics, Henan Key Laboratory of Photovoltaic Materials, Henan Normal University, Xinxiang, Henan 453007, China. E-mail:xiacongxin@htu.edu.cn*

The present supplemental material provides more details about the structural information and stability of A_2HfCh_4 (A=Ca, Sr) and Te-alloyed derivatives.

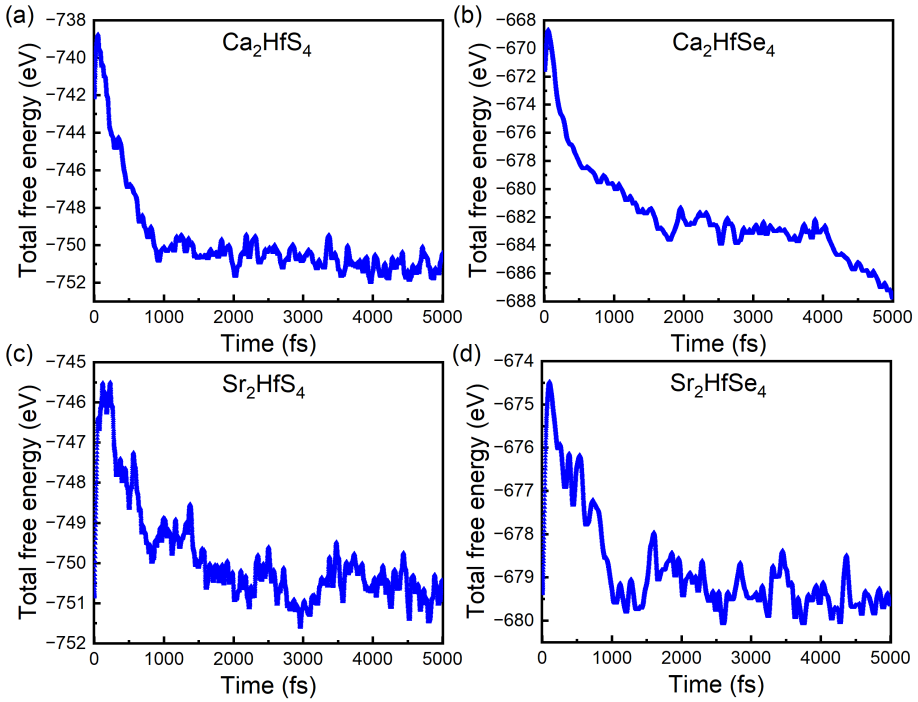

Fig. S1 Structural instability revealed by AIMD. The fluctuation of total free energy of (a) Ca_2HfS_4, (b) Ca_2HfSe_4, (c) Sr_2HfS_4, and (d) Sr_2HfSe_4 during the AIMD simulation at 300 K with a total simulation time of 5 ps and an interval of 1 fs. The significant and abrupt drop in energy observed in all four systems is a direct signature of structural collapse, providing dynamical evidence for their thermodynamic instability.

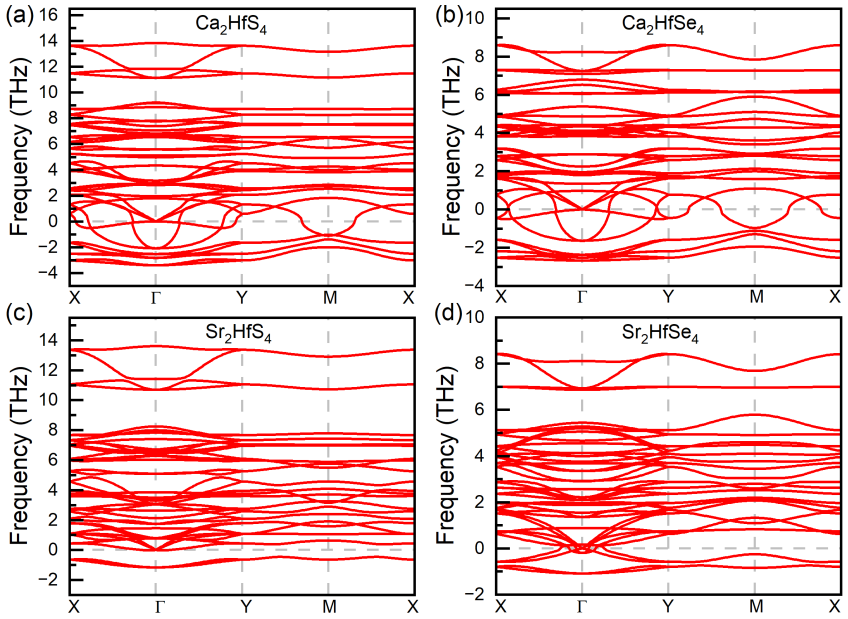

Fig. S2 Phonon dispersion spectra confirming structural instability. The spectra for (a) Ca_2HfS_4, (b) Ca_2HfSe_4, (c) Sr_2HfS_4, and (d) Sr_2HfSe_4 all exhibit significant imaginary frequencies (negative values), which is a direct signature of dynamical instability.

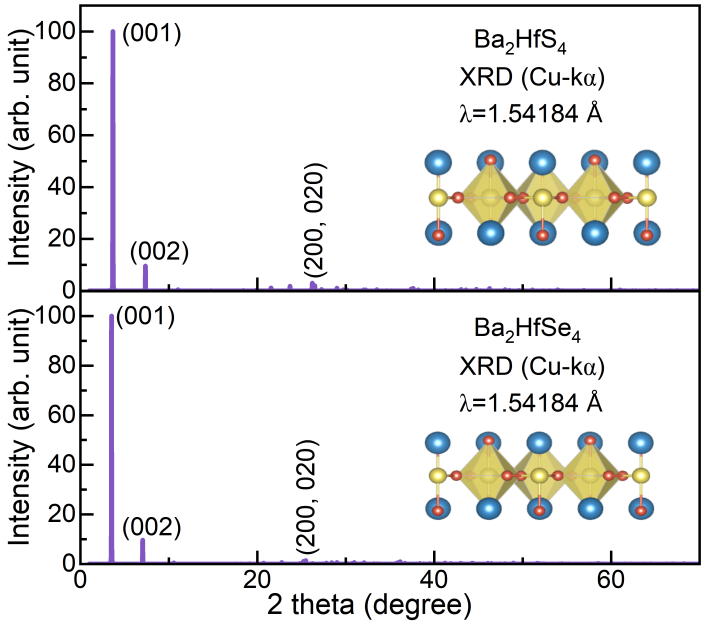

Fig. S3 The calculated XRD patterns for Ba_2HfS_4 and Ba_2HfSe_4 from 0 ° to 70° by using the radiation wavelength λ=1.54184 Å(Cu-K_α). Several important peaks are marked with the corresponding Miller indices (hkl). Inset: the relaxed structures. These patterns serve as references for experimental phase identification.

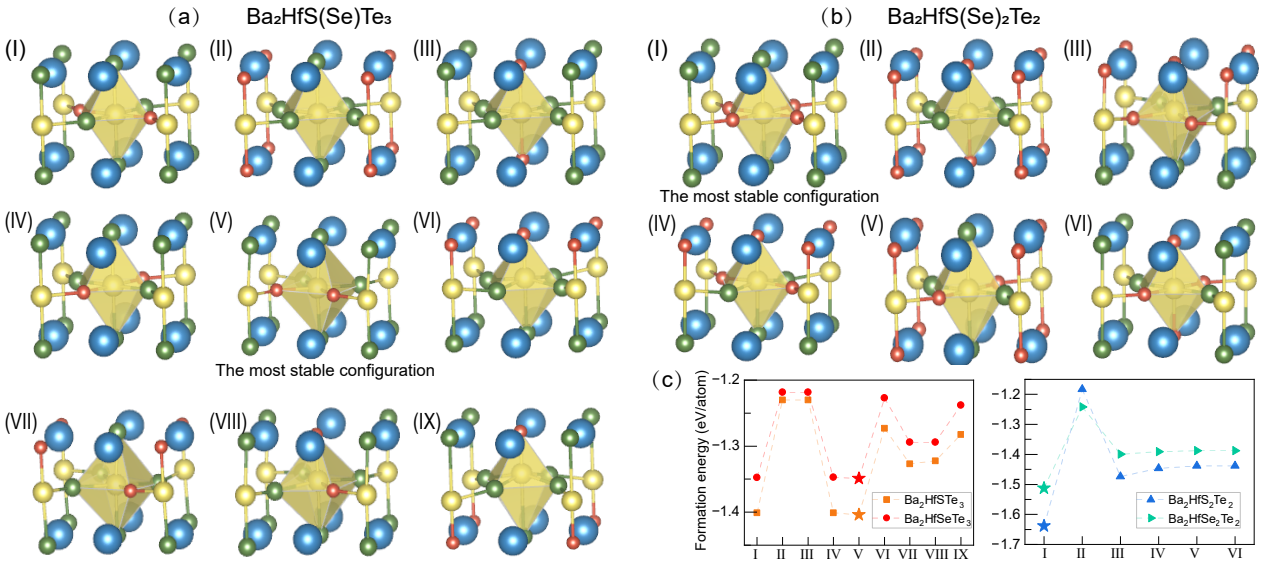

Fig. S4 Configurational exploration and relative stability of Te-alloyed structures. (a) The nine candidate doping configurations for $Ba_2HfS(Se)Te_3$. (b) The six candidate doping configurations for $Ba_2HfS(Se)_2Te_2$. (c) The calculated formation energies for all configurations shown in (a) and (b). The most thermodynamically stable configuration for $Ba_2HfS(Se)Te_3$ is Configuration *V*, and for $Ba_2HfS(Se)_2Te_2$ it is Configuration *I*. These identified lowest-energy structures are used for all subsequent electronic and optical property calculations.

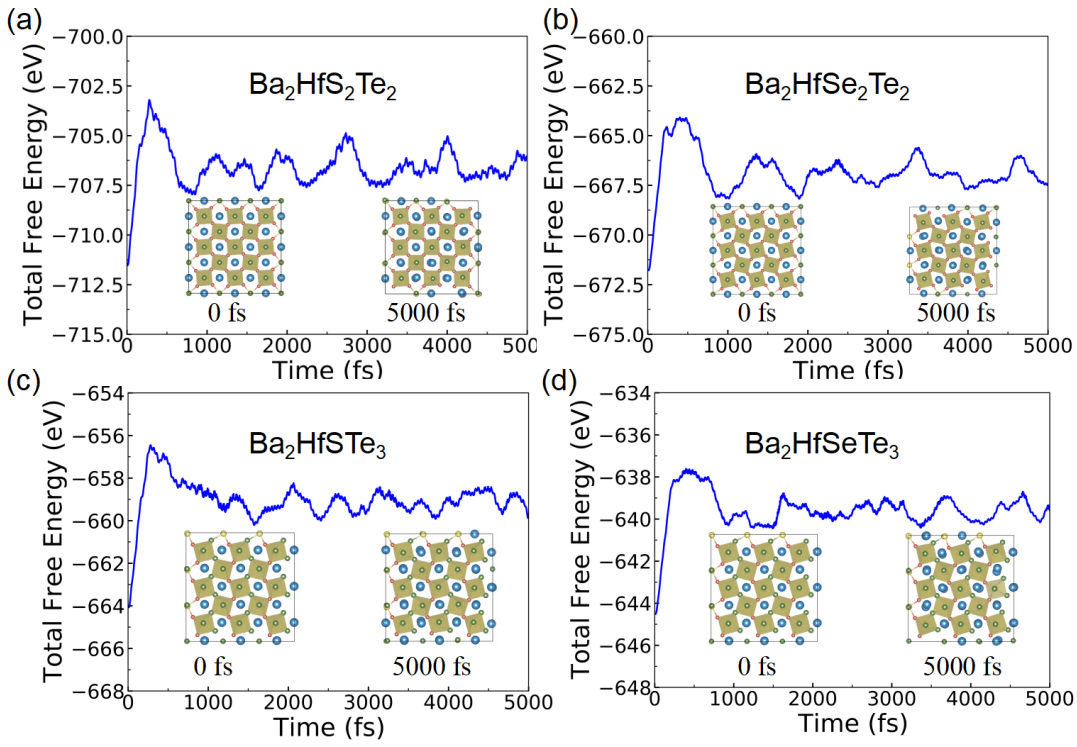

Fig. S5 The fluctuation of total free energy of (a) $Ba_2HfS_2Te_2$, (b) $Ba_2HfSe_2Te_2$, (c) Ba_2HfSTe_3 and (d) $Ba_2HfSeTe_3$ during the AIMD simulation at 300 K with a total simulation time of 5 ps and an interval of 1 fs. The insets show the initial and final crystal structure, in which the octahedral common vertex connection is well kept.

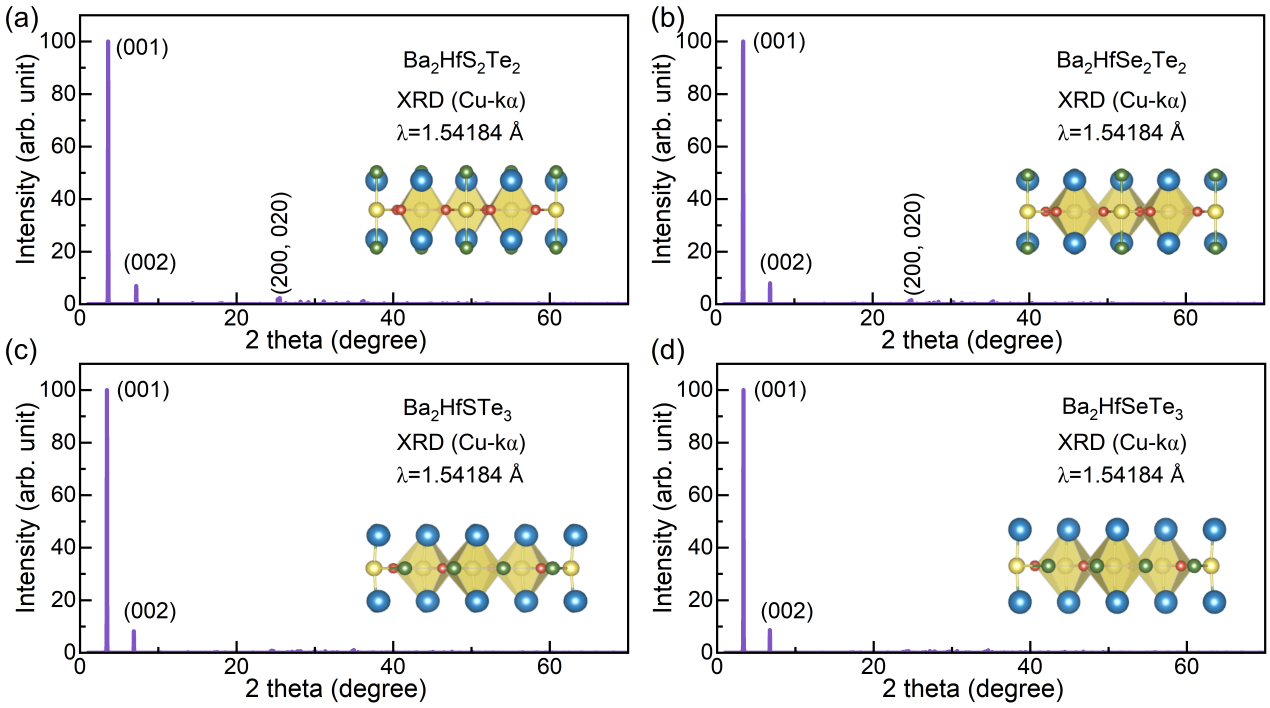

Fig. S6 The calculated XRD patterns for (a) $Ba_2HfS_2Te_2$, (b) $Ba_2HfSe_2Te_2$, (c) Ba_2HfSTe_3 and (d) $Ba_2HfSeTe_3$ from 0° to 70° by using the radiation wavelength λ=1.54184 Å(Cu-K_α). Several important peaks are marked with the corresponding Miller indices (hkl). Inset: the relaxed structures. These patterns serve as references for experimental phase identification.